Tetrahedron Letters 70 (2021) 153007

Contents lists available at ScienceDirect

Tetrahedron Letters

journal homepage: www.elsevier.com/locate/tetlet

Imaging the trace amine-associated receptor 1 by positron emission tomography

Jiyun Sun [a,b], Jiahui Chen [a,b], Katsushi Kumata [c], Zhiwei Xiao [a,b], Jian Rong [a], Ahmed Haider [a], Tuo Shao [a], Lu Wang [b], Hao Xu [b,*], Ming-Rong Zhang [c,*], Steven H. Liang [a,*]

[a] Department of Radiology, Division of Nuclear Medicine and Molecular Imaging Massachusetts General Hospital and Harvard Medical School, 55 Fruit Street, Boston, MA 02114, United States
[b] Center of Cyclotron and PET Radiopharmaceuticals, Department of Nuclear Medicine and PET/CT-MRI Center, the First Affiliated Hospital of Jinan University, Guangzhou 510630, China
[c] Department of Advanced Nuclear Medicine Sciences, National Institute of Radiological Sciences, National Institutes for Quantum and Radiological Science and Technology, Chiba 263-8555, Japan

ARTICLE INFO

Article history:
Received 19 January 2021
Revised 9 March 2021
Accepted 12 March 2021
Available online 16 March 2021

Keywords:
Trace amine-associated receptor 1 (TAAR1)
Positron emission tomography (PET)
Neuroimaging
Radiochemistry
Drug development

ABSTRACT

Trace amine-associated receptor 1 (TAAR1) has been implicated in drug addiction, schizophrenia, depression and Parkinson's disease (PD). To date, there are no reports on TAAR1-targeted probes for non-invasive quantification of receptor density in vivo. Herein, we report the synthesis of a ^{11}C-labeled TAAR1 high-affinity antagonist *N*-(3-methoxyphenyl)-6-(pyrrolidin-1-yl)-5-(trifluoromethyl)nicotinamide [^{11}C]**4** (also named [^{11}C]TAAR1-1911), as well as its physicochemical and preclinical evaluations for positron emission tomography (PET) imaging. This PET ligand was afforded using [^{11}C]CH_3I with the base NaOH in good radiochemical yield (non-decay corrected 14% relative to starting [^{11}C]CO_2), excellent radiochemical purities (>99%) and high molar activities (>37 GBq/μmol). Despite promising in vitro performance characteristics, [^{11}C]**4** did not exhibit in vivo specificity, potentially owing to fast metabolic degradation. Further studies are warranted to identify a suitable TAAR1 PET tracer, which would ultimately aid the development of TAAR1-directed therapeutic agents.

Trace amine-associated receptor 1 (TAAR1) is a G protein-coupled receptor (GPCR) that is activated by endogenous monoamines and amphetamine-related psychostimulants, including methamphetamine [1–5]. TAAR1 is widely expressed in the stomach, pancreas, intestine and the central nervous system (CNS). In the mammalian brain, TAAR1 is highly expressed in the ventral tegmental area and dorsal raphe nuclei, where it functions as a negative modulator of monoamine neurotransmission [6]. Along this line of reasoning, TAAR1 has been suggested as a potential therapeutic target for CNS and metabolic disorders, particularly owing to the implications in the pathophysiology of schizophrenia, depression, sleep disorders, Parkinson's disease, type 2 diabetes and eating disorders [7]. Several TAAR1 agonists have been shown to attenuate monoaminergic downstream signaling [3,8]. Of note, some endogenous amines and their derivatives can activate TAAR1 with nanomolar (nM) to micromolar (μM) potency [1,3,6]. While the structural scaffold of endogenous amines has been exploited for the development of TAAR1 ligands, chemical libraries of various structural scaffolds have been employed to facilitate the screening of potential drug candidates, ultimately resulting in the successful identification of highly selective and potent TAAR1 agonists (Fig. 1) [1,4,5,9,10]. In sharp contrast, the identification of promising antagonist has proven to be challenging, primarily due to the lack of selectivity of the vast majority of TAAR1 antagonists. To date, EPPTB (RO5212773) is the only well-characterized TAAR1 antagonist with high in vitro binding affinity and selectivity, as well as appropriate lipophilicity and functional activity [11,12]. EPPTB was developed by high throughput screening (HTS) and subsequent structure–activity refinements. Of note, studies with EPPTB in wild-type and *TAAR1*$^{-/-}$ mice unveiled a key regulatory mechanism of TAAR1 in dopaminergic neurons of the mesolimbic system.

Positron emission tomography (PET) is a highly sensitive and non-invasive imaging technology that allows the in vivo quantification of biological processes [13–16]. To date, a suitable TAAR1-selective probe is lacking. However, the development of a TAAR1-targeted PET radioligand would enable the non-invasive assessment of TAAR1 expression under physiological and pathological conditions, thereby shedding light on the mechanistic

* Corresponding authors.
E-mail addresses: txh@jnu.edu.cn (H. Xu), zhang.ming-rong@qst.go.jp (M.-R. Zhang), liang.steven@mgh.harvard.edu (S.H. Liang).

https://doi.org/10.1016/j.tetlet.2021.153007
0040-4039/

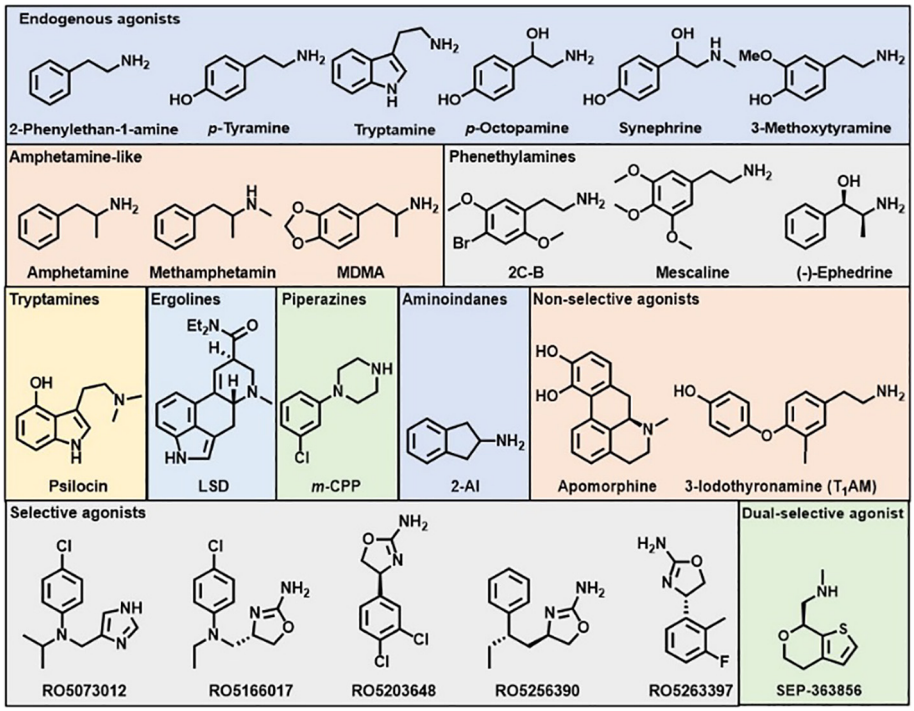

Fig. 1. Selected TAAR1 agonists.

involvement of TAAR1 in various animal disease models, as well as in patients. Further, it would accelerate the development of TAAR1 antagonists, which is a current unmet medical need. Indeed, TAAR1 antagonists harbor enormous potential for the treatment of hypodopaminergic pathologies such as Parkinson's disease [17].

Despite the high potency and selectivity of EPPTB, its chemical structure is not amenable to conventional carbon-11 labeling. In contrast, the previously reported analog, *N*-(3-methoxyphenyl)-6-(pyrrolidin-1-yl)-5-(trifluoromethyl)nicotina-mide **4**, which also demonstrated high in vitro binding affinity (K_i = 2.0 nM) [11], was suitable for ^{11}C-labeling via *O*-alkylation. Accordingly, we envisioned the development of the first TAAR1-targeted PET radioligand based on the structure of amide **4** – with the aim to allow non-invasive visualization of TAAR1 in vivo.

Target compound **4** and the respective demethylated precursor **7** were synthesized as previously reported [11], however, with minor modification as outlined in Scheme 1. Briefly, amide **4** was obtained in two steps via treatment of chloro-pyridine precursor **1** with pyrrolidine and subsequent condensation reaction with m-anisidine in an overall yield of 55% (2 steps). Similarly, precursor **7** was synthesized from intermediate acid **2** via DMAP-mediated amide formation, followed by cleavage of the protection group in an overall yield of 45% (3 steps).

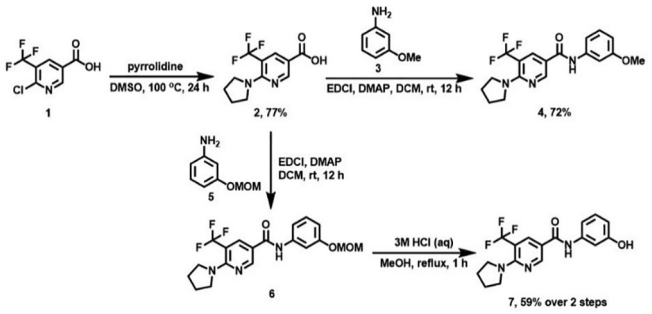

Scheme 1. Synthesis of target compound **4** and the respective precursor **7** for carbon-11 labeling.

The ADME properties and SAR of EPPTB have been previously reported, along with preliminary testing of target compound **4**, which included in vitro binding affinity and metabolism [11], In this work, we evaluated the physicochemical properties of compound **4** and predicted its blood–brain barrier (BBB) permeability using in silico predictive algorithms (CNS multiparameter optimization (CNS MPO) [18] and blood–brain barrier (BBB) Score [19]). Pharmacology and ADME results are summarized in Fig. 2. CNS MPO score and BBB score (4.62 and 4.54, respectively, using a scale of 0–6, respectively) indicated that compound **4** is a CNS-favored molecule [18,19]. The predicted ratio of C_{brain} to C_{blood} was expressed as logBB = −0.08 (ACD Percepta program), which is reasonable for brain penetration [20].

As for the assessments of metabolism and in vitro safety profiles, compound **4** exhibited a reasonably low CYP inhibition, and was found to be inactive in the hERG assay (IC50 = 10.5 μM, see Figs. S1 and S2 in Supporting Information). These encouraging results prompted us to carry on with the carbon-11 labeling of compound **4** and subsequent in vivo evaluation.

As shown in Fig. 3, the hydroxyl group of precursor **7** is accessible for conventional carbon-11 labeling with [^{11}C]CH_3I [21]. Accordingly, [^{11}C]**4** was synthesized with an automated module sequence that includes radiolabeling, purification and formulation in an overall synthetic time of 35 min. To optimize the reaction conditions, different amounts of precursor, type of base and reaction temperatures were employed, as depicted in Fig. 3A. After testing different combinations, 0.5 N NaOH(aq) in DMF at 80 °C was identified as the optimal reaction condition. The highest non-decay corrected RCY (14.0%, relative to [^{11}C]CO_2 at the end of bombardment, total synthetic time ca. 35 min) was obtained with the lowest amount of precursor **7** (Fig. 3A, entry 5). The reaction mixture was purified by semi-prep radio-HPLC to afford [^{11}C]**4** with excellent radiochemical purity (>99%) and high molar activities (37 > GBq/μmol). No radiolysis was observed up to 90 min after formulation (Fig. 3B). The in vitro stability assay (5, 30, 60 min)

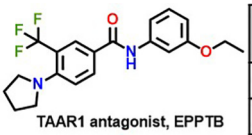

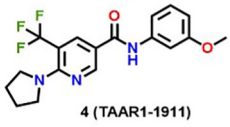

Pharmacology and Physicochemical Properties	EPPTB	4
K_i (mouse)	0.9 nM	2 nM
MW (g/mol)	378.4	365.3
TPSA [Å^2]	41.57	54.46
cLogP	4.8	3.7
HBA/HBD	4/1	5/1
Aro_R	2	2
HA	27	26
Clearance[a]	109	321

BBB Permeability of 4	
MPO score	4.621
BBB score	4.54
logBB	-0.08
CYPs and hERG IC50 of 4	
1A2	> 10 μM
2C9	5.37 μM
2C19	2.32 μM
2D6	> 10 μM
3A4	7.25 μM
hERG	> 10 μM

[a] Intrinsic clearance in mouse liver microsomes, μg/min/mg protein

Fig. 2. Summary of physicochemical and safety properties of TAAR1 antagonist EPPTB and target compound **4**.

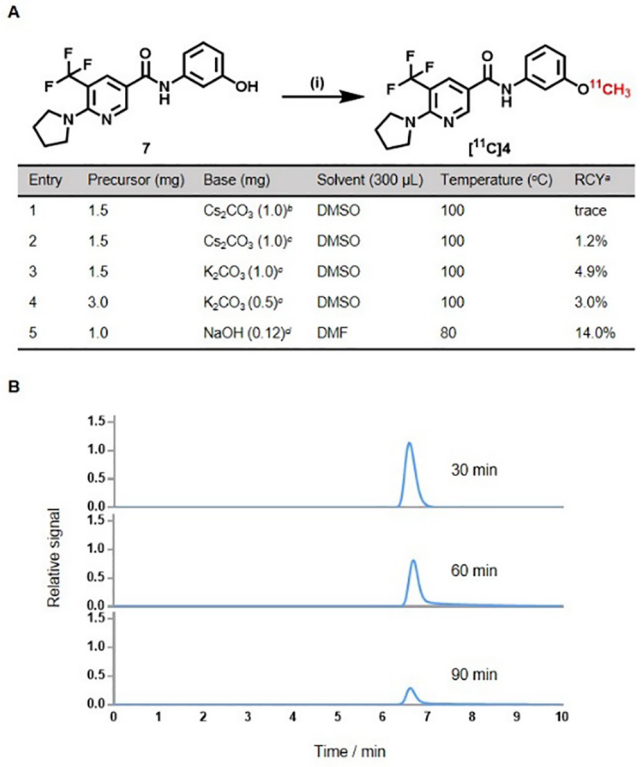

Entry	Precursor (mg)	Base (mg)	Solvent (300 μL)	Temperature (°C)	RCY[a]
1	1.5	Cs_2CO_3 (1.0)[b]	DMSO	100	trace
2	1.5	Cs_2CO_3 (1.0)[c]	DMSO	100	1.2%
3	1.5	K_2CO_3 (1.0)[c]	DMSO	100	4.9%
4	3.0	K_2CO_3 (0.5)[c]	DMSO	100	3.0%
5	1.0	NaOH (0.12)[d]	DMF	80	14.0%

Fig. 3. (A) Optimization of reaction parameters for the radiosynthesis of [^{11}C]**4**. (i) [^{11}C]MeI, DMSO, 100 °C, 5 min. [a] Non-decay corrected RCY relative to the starting activity of [^{11}C]CO_2. [b] 1.0 M aqueous solution of Cs_2CO_3 was used. [c] Solid reagent was used. [d] 0.5 M aqueous solution of NaOH was used. (B) Stability of radioligand [^{11}C]**4** in saline containing 5% of ethanol at three different time point (30, 60 and 90 min). HPLC conditions: Xselect Hss T3, 4.6 mm i.d. × 150 mm, UV at 254 nm; CH_3CN/H_2O (v/v, 70/30) + 0.1% Et_3N at a flow rate of 1.0 mL/min.

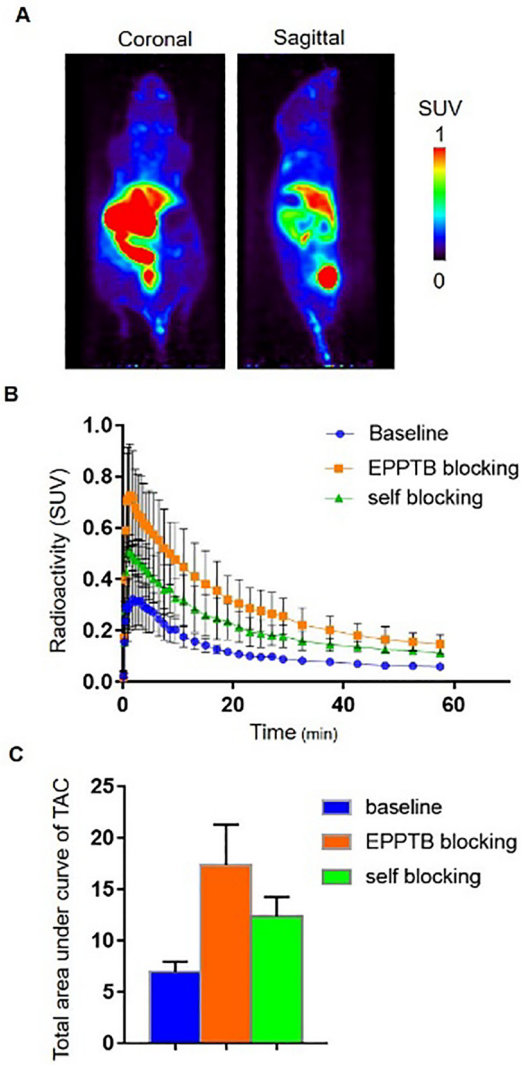

Fig. 4. (A) Representative PET images of radioligand [^{11}C]**4** (0–60 min averaged image); (B) Time-activity curves of [^{11}C]**4** in mice brain (baseline, n = 3; EPPTB blocking, 3 mg/kg, n = 3; self-blocking, 3 mg/kg, n = 2); (C) Quantification (0–60 min) using total area under curve of TAC.

proved that [^{11}C]**4** has good in vitro stability (>99% parent component) in mouse serum and blood, as well as in human serum. The lipophilicity of [^{11}C]**4** was determined by the 'shake-flask' method. As such, a $LogD_{7.4}$ valve of 3.36 ± 0.22 (n = 3) was obtained, indicating that compound **4** possesses the appropriate lipophilicity to cross the BBB.

Dynamic PET imaging with [^{11}C]**4** was carried out in CD-1 mice. Representative PET images (sagittal and coronal, averaged from 0 to 60 min), time-activity curves (TAC) and total areas under the curves of whole brain at baseline conditions are shown in Fig. 4. The limited radioactivity uptake in the whole brain (ca. 0.3 SUV at peak) indicated that [^{11}C]**4** did not reach the brain in sufficient amounts to allow appropriate TAAR1 imaging. Further, pretreatments with non-radioactive reference compound **4** or EPPTB (TAAR1 selective antagonist) resulted in higher brain uptake of [^{11}C]**4** compared to the baseline, which might be attributed to

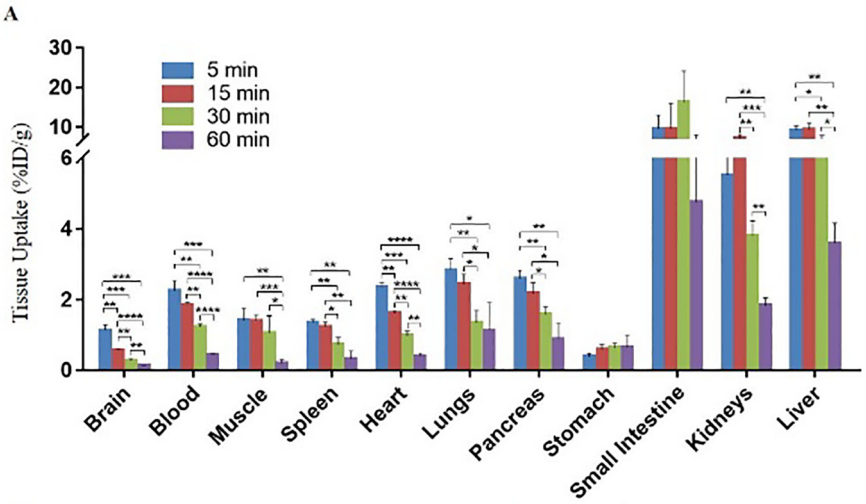

B

Time (min)		Brain Uptake (%ID/g)
5	baseline	1.13 ± 0.12
5	EPPTB blocking	1.23 ± 0.29
30	baseline	0.28 ± 0.04
30	EPPTB blocking	0.25 ± 0.14

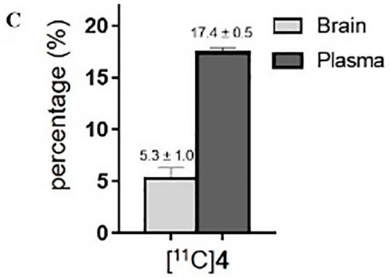

Fig. 5. (A) *Ex vivo* whole body biodistribution in CD-1 mice at four different time points (5, 10, 30 and 60 min) post injection of [^{11}C]**4**. The results are expressed as the percentage of the injected dose per gram of wet tissue (% ID/g); (B) *Ex vivo* blocking studies of [^{11}C]**4** in the mouse brain at two different time points (5 and 30 min). The blocking group were pretreated with EPPTB (3 mg/kg) for 2 min followed by [^{11}C]**4**. All data are mean ± SD, n = 3. (C) Radiometabolism in the mouse brain and plasma at 30 min post injection (n = 2). Asterisks indicate statistical significance: ****p < 0.0001, ***p < 0.001, **p < 0.01, and *p < 0.05.

several confounding factors, including nonspecific binding, increased systemic tracer availability due to the blockade of TAAR1 in peripheral organs and rapid in vivo metabolism (*vide infra*). Another explanation could be that the blocker might have resulted in a pharmacological effect that would increase cerebral perfusion and hence, delivery of the tracer (or radiometabolites) to the brain.

To verify our PET findings, ex vivo whole body biodistribution of [^{11}C]**4** was performed in CD-1 mice at four different time points (5, 15, 30 and 60 min post injection). The data are presented as the percentage of injected dose per gram of wet tissue (Fig. 5A, %ID/g). The limited brain uptake was consistent with the PET results. In contrast, high radioactivity uptake (>5% ID/g) was found in the small intestine, kidneys and liver at 5 min post injection. Further, high tracer uptake was found in the heart, lungs and pancreas. Of note, radioactivity levels in the liver reached a plateau at 5 min post injection, followed by a slow washout, thus suggesting that hepatobiliary elimination might be the primary clearance pathway. Studies were also performed under blocking conditions with EPPTB (3 mg/kg) at 5 min and 30 min time points (see Table S1 and S2 in Supporting Information for more detail). In accordance with the PET experiments, no specific binding was observed in the brain (Fig. 5B).

In vivo stability of [^{11}C]**4** was evaluated in mice at 30 min post injection. In fact, it was found that only very small fractions of the intact parent tracer were found in the brain (5.3 ± 1.0% in the brain) and in the plasma (17.4 ± 0.5%), which may explain the overall low brain uptake, as well as the high amount of nonspecific binding.

In summary, we have developed the first TAAR1-targeted PET radioligand. The [^{11}C]TAAR1-1911 ([^{11}C]**4**) was obtained with excellent radiochemical purity (>99%) and high molar activity (>37 GBq/μmol). Brain uptake, clearance and binding specificity of [^{11}C]**4** were evaluated by PET imaging, ex vivo biodistribution and radiometabolite analysis in mice. Despite the promising in vitro performance characteristics including high in silico brain penetration, low brain uptake and metabolic instability, as well as the presence of brain radiometabolites, hampered the further development of this ligand.

Declaration of Competing Interest

The authors declare that they have no known competing financial interests or personal relationships that could have appeared to influence the work reported in this paper.

Acknowledgments

We gratefully acknowledge the generous support provided by the National Natural Science Foundation of China (NO. 81901802, NO. 82071974, NO. 81871383). AH was supported by the Swiss National Science Foundation.

Appendix A. Supplementary data

Supplementary data to this article can be found online at https://doi.org/10.1016/j.tetlet.2021.153007.

References

[1] R. Zucchi, G. Chiellini, T.S. Scanlan, D.K. Grandy, Br. J. Pharmacol. 149 (2006) 967–978.
[2] E. Cichero, M. Tonelli, Future Med. Chem. 9 (2017) 1507–1527.
[3] M.D. Schwartz, J.J. Canales, R. Zucchi, S. Espinoza, I. Sukhanov, R.R. Gainetdinov, Expert Opin. Ther. Targets 22 (2018) 513–526.

[4] Z. Xu, Q. Li, Cell. Mol. Neurobiol. 40 (2020) 257–272.
[5] M. Tonelli, E. Cichero, Expert Opin. Ther. Pat. 30 (2020) 137–145.
[6] G. Rutigliano, A. Accorroni, R. Zucchi, Front. Pharmacol. 8 (2018) 1–18.
[7] M.D. Berry, R.R. Gainetdinov, M.C. Hoener, M. Shahid, Pharmacol. Ther. 180 (2017) 161–180.
[8] A.A. Aleksandrov, V.M. Knyazeva, A.B. Volnova, E.S. Dmitrieva, N.V. Polyakova, R.R. Gainetdinov, Front. Pharmacol. 10 (2019) 1–8.
[9] R.R. Gainetdinov, M.C. Hoener, M.D. Berry, Pharmacol. Rev. 70 (2018) 549–620.
[10] K.S. Koblan, J. Kent, S.C. Hopkins, J.H. Krystal, H. Cheng, R. Goldman, A. Loebel, New Engl. J. Med. 382 (2020) 1497–1506.
[11] H. Stalder, M.C. Hoener, R.D. Norcross, Bioorg. Med. Chem. Lett. 21 (2011) 1227–1231.
[12] A. Bradaia, G. Trube, H. Stalder, R.D. Norcross, L. Ozmen, J.G. Wettstein, A. Pinard, D. Buchy, M. Gassmann, M.C. Hoener, B. Bettler, Proc. Natl. Acad. Sci. U. S. A. 106 (2009) 20081–20086.
[13] S.S. Tee, K.R. Keshari, Cancer J. (United States) 21 (2015) 165–173.
[14] A. Gallamini, C. Zwarthoed, A. Borra, Cancers (Basel) 6 (2014) 1821–1889.
[15] P. Brust, J. van den Hoff, J. Steinbach, Neurosci. Bull. 30 (2014) 777–811.
[16] W. Mier, D. Mier, Front. Hum. Neurosci. 9 (2015) 1–6.
[17] A. Alvarsson, X. Zhang, T.L. Stan, N. Schintu, B. Kadkhodaei, M.J. Millan, T. Perlmann, P. Svenningsson, J. Neurosci. 35 (2015) 14057–14069.
[18] T.T. Wager, X. Hou, P.R. Verhoest, A. Villalobos, ACS Chem. Neurosci. 1 (2010) 435–449.
[19] M. Gupta, H.J. Lee, C.J. Barden, D.F. Weaver, J. Med. Chem. 62 (2019) 9824–9836.
[20] D.E. Clark, J. Pharm. Sci. 88 (1999) 815–821.
[21] X. Deng, J. Rong, L. Wang, N. Vasdev, L. Zhang, L. Josephson, S.H. Liang, Angew. Chem. Int. Ed. 58 (2019) 2580–2605.